

RESEARCH PAPER



LRRK2 binds to the Rab32 subfamily in a GTP-dependent manner *via* its armadillo domain

Emma McGrath ^{a,b,*}, Dieter Waschbüsch^{a,*}, Brian M. Baker^b, and Amir R. Khan ^a

^aSchool of Biochemistry and Immunology, Trinity College Dublin, Dublin, Ireland; ^bDepartment of Chemistry and Biochemistry, University of Notre Dame, Notre Dame, IN

ABSTRACT

LRRK2 is a multi-domain Ser/Thr kinase that is associated with inherited and sporadic cases of Parkinson's disease. Many mutations linked to disease are associated within a central ROC-COR regulatory region and the subsequent kinase domain, leading to enhanced catalytic activity. The N-terminus of human LRRK2 consists of armadillo repeat motifs (ARMs) followed by ankyrin repeats (ANKs). Recently, Rab GTPases have emerged as key players in LRRK2 function, both as substrates of the kinase, and as regulators of the catalytic activity. Rabs recruit effector proteins *via* their GTP-dependent switch 1 and 2 regions to distinct sub-cellular compartments to regulate membrane trafficking. LRRK2 phosphorylates Rab8, Rab10 and Rab12 in switch 2, and this activity is regulated *via* interactions with Rab29. Furthermore, the related Rab32-subfamily GTPases, Rab32 and Rab38, have also been shown to interact with LRRK2. Here, we have mapped the interactions of the Rab32-subfamily to the ARM domain of LRRK2. The complexes are dependent on the GTP state of the Rabs *in vitro*, implying that LRRK2 may be an effector of the Rab32-subfamily of small GTPases. X-ray crystal structures of the Rab32-family GTPases and subsequent mutational studies reveal that a positively charged residue in switch 1 is critical for binding of Rab32/38 to LRRK2. Homology modelling and mutational analyses of the ARM domain point to a patch of negatively charged residues that contribute to complex formation. These structural and biochemical studies provide a framework for understanding the molecular basis for Rab regulation of LRRK2 and its role in Parkinson's disease.

ARTICLE HISTORY

Received 28 June 2019
Revised 26 August 2019
Accepted 2 September 2019

KEYWORDS

Rab GTPases; leucine-rich repeat kinase 2; membrane trafficking; X-ray crystallography; Rab32 subfamily; biophysics

Introduction


Parkinson's disease (PD) is a disorder of the central nervous system that manifests as a progressive degeneration of motor mobility, balance, and tremors. Features of the pathology include loss of dopaminergic neurons in the mid-brain and the presence of protein aggregates termed Lewy bodies, composed mainly of α -synuclein, in surviving neurons [1]. About 10% of cases have a genetic basis, with the most common gene being the *Leucine-Rich Repeat Kinase 2 (LRRK2)* [2]. The gene product is a 2,527-residue (286kDa) protein with multiple domains belonging to the ROCO family that is involved in regulation of autophagy, mitochondria, and Golgi dynamics [3]. The kinase domain, located near the C-terminus, phosphorylates itself and other proteins at serine/threonine residues [2,4,5]. Preceding the kinase domain, there is a Ras-like ROC domain (Ras of complex) followed in tandem by a COR domain (C-terminal of Ras). The ROC domain binds to nucleotide (GTP/GDP) and is distantly related to the Rab family of small GTPases. The ROC-COR tandem

domains regulate LRRK2 activity and numerous missense mutations have been localized to these regulatory and kinase domains [6–8]. In addition to early onset forms of PD associated with autosomal dominant mutations, LRRK2 is also linked to late-onset and sporadic cases of PD [9].

Insight into LRRK2 functions has progressed significantly with the finding that a subset of small GTPases that include Rab8 and Rab10 are physiological substrates of the enzyme [5,10]. Rabs comprise the largest (~70) members of the Ras superfamily, and they cycle between an active GTP-bound and inactive GDP form to regulate membrane trafficking in eukaryotic cells [11]. Active Rabs migrate to distinct sub-cellular compartments where they recruit cytosolic effector proteins. The 'switch' regions of Rabs, termed switch 1 and 2, undergo local conformational changes that enable recruitment of GTP-specific effectors, which subsequently control processes such as vesicle formation/fusion, motility, and other aspects of cell dynamics [12]. LRRK2 phosphorylates

CONTACT Amir R. Khan  amirrafk@tcd.ie  School of Biochemistry and Immunology, Trinity College Dublin, Dublin 2, Ireland

*These authors contributed equally to this manuscript.

 Supplemental data for this article can be accessed [here](#).

© 2019 Informa UK Limited, trading as Taylor & Francis Group

Rab8 and Rab10 at conserved threonine residues in the switch 2 region and the post-translational modification modulates interactions between Rabs and their binding partners [5]. For example, phosphorylated Rab8 and Rab10 interact with RILPL2 (Rab interacting lysosomal like protein 2) leading to ciliogenesis [13], a process that may be affected in LRRK2-dependent neuronal pathologies. Upstream of the enzymatic function, Rab29 (Rab7L1) recruits LRRK2 to Golgi and activates the kinase, leading to enhanced phosphorylation of Rab8 and Rab10, as well as increased autophosphorylation [14]. Rab32 is not a target for the kinase but it interacts with LRRK2 and regulates its sub-cellular localization [15]. Thus, LRRK2 is at the centre of a Rab signalling cascade that is a key to understanding the biological functions of LRRK2 and its relationship to PD.

Functional studies of Rab29-mediated LRRK2 activation, as well as co-immunoprecipitation analyses, have implied that Rab29 binds to the ANK domain of LRRK2 [14,16]. A previous study that used the T21N (GDP-locked) and Q67L (GTP-locked) mutants of Rab29 suggested that both forms could bind LRRK2 [17]. However, in contrast to other Rab GTPases, these same authors find that the QL mutant of Rab29 behaves in a dominant-negative fashion [18]. Given the complications in studying nucleotide-dependence for LRRK2 binding in cells, it would be advantageous to perform *in vitro* analyses of purified Rab29:LRRK2 complexes. Molecular details of Rab29:LRRK2 interactions are essential for an understanding of the mechanism by which LRRK2 kinase activity is stimulated by Rab29 and the effects of pathogenic LRRK2 variants. Rab29 belongs to the Rab32-subfamily of small GTPases (Rab29, Rab32 and Rab38; Interpro IPR030697) and shares 56% identities (77% similarities) to Rab32 within their G-domain fold. Rab32 and Rab38 are redundant in function and have been classically linked to melanosome biogenesis, while Rab29 regulates trafficking at Golgi compartments.

Here we show that Rab32-subfamily (Rab29, Rab32 and Rab38) interact with LRRK2 in a GTP-dependent manner. Thus, LRRK2 may be an effector of the Rab32-subfamily of small GTPases. Crystal structures of active Rab32 and Rab38, together with mutational analyses, reveal that abolition of a positive charge in switch 1 (R39Q in Rab38) is critical for binding to LRRK2. Interestingly, the equivalent mutation in Rab29 (K39Q) is dispensable for binding, suggesting subtle distinctions between Rab32/38 and Rab29 interactions with LRRK2. A Rab32-subfamily binding site on LRRK2 has also been narrowed to the C-terminal half of the ARM domain. Exploiting a combination of homology modelling, mutagenesis, pulldowns and

fluorescence-based assays, we find that a negatively charged loop in the ARM domain contributes to complex formation with Rab GTPases.

Materials and methods

Rab expression constructs

The cDNA corresponding to human Rab38 (residues 1–181 of 211) was synthesized (Genscript, Piscataway, NJ, USA) and inserted into pET15b at the NdeI-BamHI site. The translated protein contains an N-terminal His₆-tag followed by a thrombin cleavage site. Following thrombin cleavage, the recombinant protein contains the non-native sequence Gly-Ser-His at the N-terminus, preceding the first methionine residue of Rab38. Mutagenic oligonucleotides used to generate Rab38 mutants in this vector are listed in Table S1. Human Rab32 Q85L region 20–198 of 225, corresponding to the G-domain, was cloned into pNIC28-Bsa4 using ligation-independent cloning methods. The forward primer was 5'-ACTTCCAATCCATGGAGACCCGCGAGCAC-3' (Met1 underlined), and the reverse primer was 5'-TATCCACCTTTACTGTTAGCTTTGGTGGTTTACAAGA-ATC-3' (STOP codon underlined). The template for the PCR reaction was obtained from the lab of Prof. Angelika Barnekow (University of Münster, Germany). We also made a Rab32 Q85L residues 1–198 construct using the same template. Forward primer was 5'-TACTTCCAATCCATGGCGGGCGGAGGAGCC-3', reverse primer 5'-TATCCACCTTTACT-GTTAGCTTTGGTGGTTTACAAGA-ATC-3'. The G-domain of human Rab29 (residues 1–177 of 203) was also LIC cloned into the pNIC28-Bsa4 vector. The forward Primer was 5'-TACTTCCAATCCATGGGCAGCCGCGACCACC-3', the reverse primer was 5'-TATCCACCTTTACTGTTAGGATTCTCATCATCTTTTCAATG-3'. The template for the PCR reaction was obtained from the lab of Prof. Dario Alessi (University of Dundee, DU50261).

LRRK2 expression constructs

Codon-optimized cDNA corresponding human LRRK2 (1–910) from Genscript (Piscataway, NJ, USA) was inserted into pET15b (Novagen). This region of LRRK2 comprises the full ARM and ANK domains, with an N-terminal His₆ tag and a thrombin cleavage site. A variant of this construct with mutations in non-conserved cysteine residues to optimize solubility was also generated: C6S, C9S, C228S, C236S, C272S, and C746A (LRRK2^{Cmut}).

From the above ARM-ANK (1–910) constructs, the region 10–661 (LRRK2⁶⁶¹) was amplified and inserted into pNIC28-Bsa4. This segment covers the complete armadillo domain of LRRK2. It was amplified by PCR using the following primers: 5'-TACTTCCAATCCATGGAGGAAG-ATGAGGAAACCC-3' (forward) and 5'TATCCACCTTTACTGTAAACGGTTCAGCGCCG-CCAGC-3'. A deletion variant of LRRK2⁶⁶¹ (Δ CC) lacking the residues 330–345 were made by a two-step PCR using the following primers: 5'-TACTTCCAATCCATGGAGG-AAGATGAGGAAACCC-3' (PCR1 forward; same as for the 10–661 construct); 5'-CCAAAACAGTTTGCCCGTCGTACCCAGATCCTGGTTCAGGAAA-ATG-3' (PCR1 rev; the inserted linker replacing residues 320–345 is underlined); 5'-CAG GAT CTG GGT ACG ACG GGC AAA CTG TTT TGG CTG GAG GCG-3' (PCR2 for; the inserted linker replacing residues 330–345 is underlined); 5'-TATCCACCTTTACTGTAAACGGTTCAGCGC-CGCCAGC-3' (PCR2 rev; same as for the 10–661). The final Δ CC insert was then LIC cloned into the pNIC28-Bsa4 vector. The LRRK2 1–910 L728D +L729D was generated serendipitously while performing site directed mutagenesis to obtain a L729D single mutant using the following primers: forward: 5'-CATGGTGGAAATGCCTGGATCTGCTGGGTGCTGAC-3'; reverse: 5'-GTCAGCACCCA-GCAGATCCAGGCATTCCACCATG-3'. The template for the L728D +L729D mutation was LRRK2-WT (1–910) with a codon-optimized sequence for expression in *E.coli*. The primers used were: forward: 5'-TACTTCCAATCCATGGCGAGCGGTAGCTGCC-3'; reverse: 5'-TATCCACCTTTACTGT-TAGCTGTTGCTCTTTTCTTAACC-3'. The resulting sub-clones were inserted by LIC into the pNIC28-Bsa4-vector. We also used a LRRK2 WT (1–910) template to generate a minimal ARM domain, residues 1–552 (LRRK2⁵⁵²). This vector was the template for the generation of several site-directed mutants, which are listed in Table S2. All constructs generated by PCR were confirmed by DNA sequencing.

Expression and purification of proteins

The following protocol was utilized for expression of all His-tagged proteins. Expression was carried out in 2xYT Broth supplemented with 34 μ g/ml kanamycin (FORMEDIUM™) at 37°C. At an OD₆₀₀ of 0.7 the culture was transferred to 18°C incubators for 20 min before induction with 0.1 mM IPTG for 18 hours. Cells were harvested by centrifugation and the pellets were resuspended in His-tag extraction buffer (20 mM Tris-HCl, 300 mM NaCl, 5 mM MgCl₂, 20 mM

imidazole and 10 mM β -mercaptoethanol, pH 8.0). Following sonication and centrifugation, the lysate was loaded onto Ni²⁺-agarose resin and washed with extraction buffer in step gradients with up to 40 mM supplemental imidazole (pH 8 for all solutions). Rabs were eluted in extraction buffer (20 mM Tris-Cl, 100 mM NaCl, 5 mM MgCl₂, 1 mM DTT, pH 8) supplemented with 200 mM imidazole, and then dialysed overnight (extraction buffer) in the presence of proteolytic enzyme (either rTEV or thrombin, depending on the construct). The cleaved proteins were run a second time through Ni²⁺-agarose resin and the flow-through fractions were collected and dialysed in low-salt buffer (20 mM Tris-Cl, 10 mM NaCl, 5 mM MgCl₂, 1 mM DTT, pH 8). Proteins were loaded onto a Mono-Q column (5/50 GL, GE Healthcare) and eluted with a gradient up to 600 mM NaCl. Peaks were directly loaded onto a Superdex-75 gel filtration column (GE Healthcare), eluted in 20 mM Tris-Cl, 100 mM NaCl, 1 mM DTT and 5 mM MgCl₂ (pH 7.5).

Expression of LRRK2 proteins was performed using the same protocols as above. For some experiments, purification was halted after the first Ni²⁺-agarose purification step (uncleaved His₆ tag).

Rab nucleotide exchange reaction

In order to generate active or inactive Rabs, proteins at 1 mg/mL concentrations were incubated in 10 mM EDTA for 10 minutes at room temperature in the presence of 10X molar excess nucleotide (GppNHp or GDP, as required). The exchange was terminated by addition of 15 mM MgCl₂ and excess nucleotides were removed by running samples through a PD10 column (GE healthcare), or by immediate gel filtration chromatography. For fluorescence studies *N*-methylanthraniloyl (mant) derivatives of GppNHp and GDP were used for nucleotide exchange, following the same protocol. Rabs were concentrated to 10 μ M for fluorescence assays, and 50–300 μ M for pulldowns and crystallization trials. Protein concentrations were calculated based on their A₂₈₀ using a ND-1000 NanoDrop Spectrophotometer (Thermo Scientific).

Isothermal titration calorimetry (ITC)

Experiments were performed using an ITC-200 calorimeter (Malvern Instruments). Proteins were dialysed together in buffer (10 mM Tris-Cl, 100 mM NaCl, 5 mM MgCl₂, and 1 mM DTT, pH 7.5) to minimize heats from buffer mismatch. Samples were centrifuged at 13,200 rpm for 10 minutes prior to the experiments. Typical concentrations of proteins for the injections were

300–600 μM Rab GTPase placed in the syringe, titrated into 30–60 μM LRRK2. All titrations were performed at 293K. Data were processed using Origin 7.0 software.

Fluorescence assays

Fluorescence measurements to obtain quantitative binding data were carried out at 20°C (293K) in a buffer containing 20 mM HEPES pH7, 100 mM NaCl, 5 mM MgCl_2 , 1 mM DTT, using established techniques[19]. A final concentration of 0.5–1 μM mant-GppNHp/GDP bound Rab proteins were incubated with increasing concentrations of LRRK2 1–552 WT in 80 μL volumes. Background fluorescence of mant-GppNHp associated Rab GTPases in the absence of LRRK2 was subtracted and non-linear regression curve fitting and dissociation constant (K_d) determination was performed using GraphPad Prism 8 software. Typically, samples of 0.5 μM Rab (mant-GppNHp) were incubated with increasing concentrations of LRRK2 1–552 and anisotropy was measured with the SpectraMax M5 plate reader. The experiment was designed using the preconfigured 'Fluorescence Polarization' protocol within the SoftMax Pro software. The mant fluorophore was excited at 355 nm and emission was detected at 448 nm. Background fluorescence of Rab GTPases in the absence of LRRK2 was subtracted from readings to obtain the change in anisotropy (Δr) upon complex formation. Inactive forms of the Rab32 subfamily bound to mant-GDP and Rab11(mant-GppNHp) which does not interact with LRRK2 were used as controls.

To analyse the relative effects of mutations on binding, multiple measurements were taken at a fixed 10 μM concentration of LRRK2 with 1 μM Rab(mant-GppNHp) protein and the change in fluorescence plotted as a bar graph using GraphPad Prism 8 software. Rab (mant-GDP) and Rab11(mant-GppNHp/GDP) signals were also measured as controls. These concentrations were chosen since they provide a clear contrast between the Rab32 subfamily and a control, such as Rab11.

In vitro pulldowns of Rabs and LRRK2

His₆-tagged Rabs (GTP, GppNHp or GDP) comprising the G-domains were used to pulldown untagged LRRK2. The proteins were mixed together in 1.5 mL centrifuge tubes with 25 μL Ni²⁺-agarose resin in a final volume of 1 ml of binding buffer (20 mM Tris pH8.0, 300 mM NaCl, 20 mM Imidazole, 5 mM MgCl_2 , 10 mM β -mercaptoethanol). The reaction mixture was subjected to mild shaking for 15 minutes. Following gentle

centrifugation (1,000 rpm), the resin was washed 3 times with 1 ml of the binding buffer. Following release of proteins from resin with 50 μL elution buffer (20 mM Tris-Cl pH8.0, 300 mM NaCl, 200 mM imidazole), samples were subjected to SDS-PAGE and visualization with 0.5% Coomassie Brilliant Blue.

Crystallization of Rab Gtpases

Rab32(Q85L), Rab38(Q69L) and Rab29 WT were purified by Ni²⁺-agarose, ion-exchange, and gel filtration chromatography, as described above. Rab32 crystals were grown in 0.2M sodium potassium tartrate, 0.1M Bis-Tris propane pH 8.5, 20% w/v PEG 3350. Rab38 crystals were grown in 0.2M potassium thiocyanate, 0.1M sodium cacodylate pH6.5, 15% PEG 4000. Rab29 crystals were grown in 2M NaCl, 0.1M HEPES pH 7. Rab29 contained the mutations C84A+C120A+C127S to improve crystal quality following initial hits. Crystallization trials were performed by the sitting drop vapour diffusion method in a 1:1 ratio with reservoir using 5–10 mg/mL protein concentrations. No exogenous nucleotides were added during crystallization trials. Crystals were harvested and cryoprotected using reservoir solution supplemented with 25% glycerol and flash frozen in liquid nitrogen at 77K.

Structure determination and refinement

X-ray diffraction data were indexed using XDS and scaled with Aimless [20,21]. The structure of Rab32(GTP) was solved by molecular replacement using the structure of Rab32 in its complex with VARP [PDB code 4cym, ref [22]]. The structure of Rab29 and Rab38 were subsequently solved using the refined structure of Rab32. Alternate cycles of model fitting and refinement were performed using the software Coot and Phenix [23,24]. Data collection and refinement statistics are provided in Table 1. The co-ordinates have been deposited in the Protein Data Bank.

Homology modelling of the ARM domain

The amino acid sequence of LRRK2 (1–552) was aligned to sequences of known armadillo domains using the Consensus and Homology suites in the software MOE [25]. Despite a similar 3-D fold, sequence identities are less than 15% overall, therefore it was critical to identify the short α -helical motifs predicted from secondary structure predictions. The ARM domain of β -catenin [Protein Data Bank (PDB) code 4evp] was ultimately used to thread the sequence of LRRK2 into the armadillo fold. Previously described correlations between sequence and the armadillo motifs of LRRK2 were also used to guide the structural

Table 1. Data collection and refinement statistics.

	Rab29(GDP)	Rab32(GTP)	Rab38(GTP)
Data collection			
Beamline	24-ID-C, APS	Proxima 2A	Proxima 2A
Detector	Pilatus 6M-F	ADSC	Eiger 9M
Space group	P3 ₁ 21	P4 ₃	P2 ₁
Unit cell lengths (Å)	71.96, 71.96, 86.35	53.66, 53.66, 129.78	70.04, 70.99, 74.49
Unit cell angles (°)	90, 90, 120	90, 90, 90	90, 102.21, 90
Asymmetric unit	1	2	4
Wavelength (Å)	0.98	0.98	0.98
Low resolution limit (Å)	86.35 (1.47)	41.35 (2.19)	49.28 (1.83)
High resolution limit (Å)	1.45	2.13	1.79
Total No. reflections	450,712 (18,782)	84,873 (6884)	455,161 (20,319)
Unique reflections	46,405 (2,211)	20,365 (1646)	66,651 (3,593)
Multiplicity	9.7 (8.5)	4.2 (4.2)	6.8 (5.7)
Completeness (%)	99.6 (93.5)	97.6 (99.7)	98.7 (83.2)
Wilson B-factor (Å ²)	21.8	34.5	20.1
R _{merge} (%)	5.2 (163.1)	7.4 (89.1)	7.5 (65.2)
R _{meas} (%)	5.5 (173.6)	8.4 (102)	8.2 (71.8)
Mn(I) correlation CC(1/2)	1.0 (0.68)	0.998 (0.59)	0.999 (0.867)
I/σ all data	27.4 (1.4)	12.4 (1.5)	12.9 (2.4)
Refinement statistics			
Model (chain/residues)			
A	4–177	20–198	1–131, 142–181
B		20–196	1–131, 143–180
C			1–131, 142–181
D			1–131, 142–181
Ramachandran map (%)			
Favourable+allowed	98.26	100	100
Outliers	0	0	0
R _{work} /R _{free} (%)	16.51/18.43	19.07/22.32	19.02/21.23
Non-hydrogen atoms			
Protein	1396	2,775	5,587
Ligands	34	66	132
Mg ²⁺	1	2	4
Waters	194	50	700
Mean isotropic B-factor (Å ²)	29.38	38.6	25.0
R.m.s. deviations			
Bond lengths (Å)	0.02	0.018	0.005
Bond angles (°)	1.63	1.92	1.15
PDB code	6hh2	6ff8	6hdu

Values in parentheses correspond to the statistics for the highest resolution. Data collection was performed at APS, Advanced Photon Source (NECAT, 24-ID-C); Proxima 2, Soleil Synchrotron, France. $R_{\text{merge}} = \sum_{\text{hkl}} \sum_j |I_{\text{hkl},j} - \langle I_{\text{hkl}} \rangle| / \sum_{\text{hkl}} \sum_j I_{\text{hkl},j}$; $R_{\text{meas}} = \sum_{\text{hkl}} \{N(\text{hkl})/[N(\text{hkl})-1]\}^{1/2} \times \sum_j |I_{\text{hkl},j} - \langle I_{\text{hkl}} \rangle| / \sum_{\text{hkl}} \sum_j I_{\text{hkl},j}$; Refinement residuals (R-factors), $R = \sum_{\text{hkl}} |F_{\text{o,hkl}} - F_{\text{c,hkl}}| / \sum_{\text{hkl}} F_{\text{o,hkl}}$.

alignment [26]. An energy minimization was performed to relieve mild steric repulsions. An independent model of the ARM domain using the Swiss Model 3D server and the structure of importin (PDB code 1 ukl) resulted in a similar overall 3-D model, with the core helical motifs relatively conserved and modest changes in the size of the connecting loops (data not shown).

Analytical HPLC analyses of nucleotides

The G-domains of the Rab GTPases were purified as described above. Proteins were boiled for 10 min at 95°C to release the nucleotide, followed by centrifugation for 30 min 16,000xg, 4°C to remove precipitated protein. The supernatant was mixed with running buffer (100 mM potassium phosphate, 8 mM tetrabutylammonium acetate, pH 6.5) at a 1:1 ratio. The samples were loaded on an Acquity Ultra Performance system (Waters Corporation, Milford, MA, USA; or Varian 920 LC machine, Agilent, Stockport, UK) equipped with a ZORBAX 300SB-C18

column (Agilent, Stockport, UK). In order to verify the nucleotide state of Rabs from elution profiles, pure solutions of GMP, GDP, GTP (Sigma Aldrich) and GppNHp (Jena Bioscience, Germany) were subjected to HPLC and compared with the samples from proteins.

Results

Rab29 binds to the ARM domain of LRRK2 in a GTP-dependent fashion

The interactions between Rab29, Rab32 and Rab38 with LRRK2 were investigated using pulldown assays with purified proteins *in vitro* (Figure 1). Rabs were expressed as truncations lacking the C-terminal tail (G-domain only) to enable purification of milligram amounts of proteins. As evidenced by numerous crystal structures of Rab:effector complexes, the G-domain encompasses the region necessary for effector interactions, but additional contributions cannot be ruled out from the hypervariable regions. Rabs were purified as

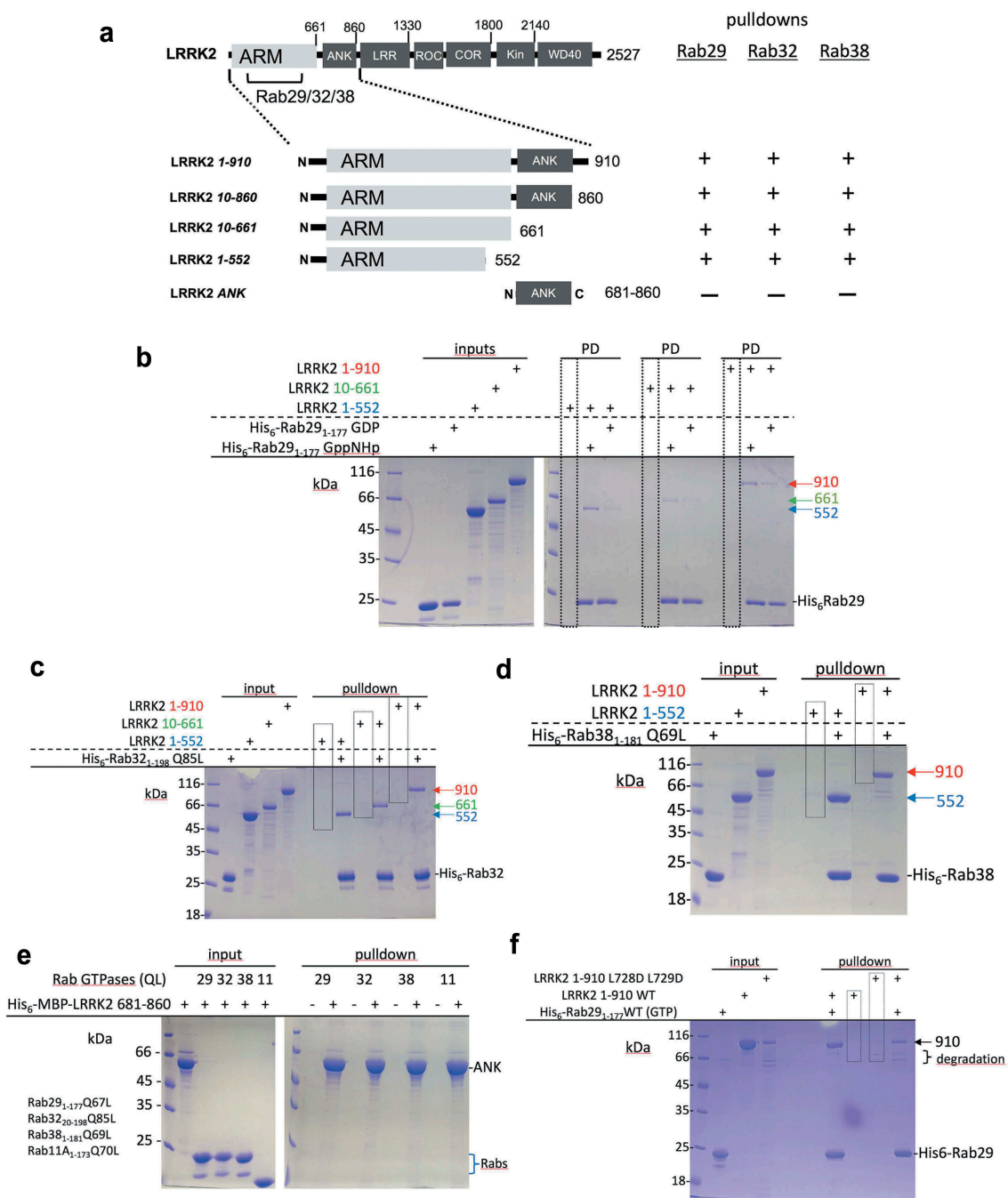


Figure 1. Rabs interact with the ARM domain in a GTP-dependent manner.

(a) LRRK2 domains used in the pulldowns and their interactions with Rab GTPases. (b) Pulldowns of various LRRK2 fragments by Rab29. Input proteins are on the left, while pulldowns (PD) are organized towards the right side of panels. (c) Rab32 pulldowns of various LRRK2 fragments. (d) Rab38 pulldowns of LRRK2. (e) Rab pulldowns of the ANK domain, suggesting no significant interactions. (f) Rab29 pulldown of LRRK2 harbouring Leu→Asp mutations in the ANK domain. Despite partial degradation of this mutant, the pulldown reveals that Rab29 retains binding affinity to the intact fragment (1–910; L728D+L729D). Some of the negative control lanes are shown in boxes to emphasize the contrast in pulldowns.

active (GTP, GppNHp) or inactive (GDP) forms. Nucleotide exchange was confirmed using HPLC analyses of purified proteins (Suppl Figure S1). Various deletion mutants of LRRK2 were expressed in order to identify the domains that interact with the Rab32-

subfamily. Variants of the ARM and ANK domains with selected Cys residues mutated to Ser and Ala (LRRK2^{WT} and LRRK2^{Cmut}) revealed no apparent differences in binding of the to Rab GTPases (Suppl Figure S2), therefore they could be used

interchangeably for pulldown studies. A summary of the pulldowns is shown in Figure 1(a).

The pulldown of LRRK2 by His₆-tagged Rab29 is dependent on the GTP form of the small GTPase (Figure 1(b)). The pulldown panels reveal a higher intensity of LRRK2 relative to the GDP form. The negative controls are also included and correspond to a pulldown of untagged LRRK2 by Ni²⁺-agarose beads. These *in vitro* data suggest that LRRK2 may be an effector of Rab29. In addition, Rab29 interacts robustly with the ARM domain (1–552), implying that at least one binding site is within the armadillo repeats of LRRK2. Further repetitions of Rab29 pulldowns of LRRK2 are shown in Suppl Figure S3. The GTP-locked (QL) variants of Rab32 and Rab38, which comprise the Rab32-subfamily of small GTPases together with Rab29, also interact with the minimal ARM domain of LRRK2 (Figure 1(c–d)). There are no interactions observed between any of the Rabs and the purified ANK domain (Figure 1(e)).

We also used our *in vitro* strategy to assess previous models of the interactions between Rab29 and LRRK2 in human cell lines [14,16]. Published cellular studies involving co-expression of Rab29 with a LRRK2 variant harbouring mutations in the ANK domain (L728D+L729D) led to a dramatic loss of LRRK2 membrane association, relative to WT [14]. These observations and other markers of LRRK2 activation had implied that Rab29 may bind directly to the ANK domain [14,16]. Therefore, we generated a recombinant LRRK2 variant (1–910, L728D+L729D) and performed a direct pulldown *in vitro* (Figure 1(f)). The mutations in the ANK domain significantly destabilized the *E.coli*-expressed protein, but sufficient amounts of intact product were obtained for the pulldown assay. Rab29(GTP) retains the ability to bind mutant L728D+L729D, which is consistent with a binding site in the unaffected ARM domain. However, additional interactions between Rab GTPases and domains of LRRK2 downstream of the ARM domain cannot be ruled out by these *in vitro* analyses.

Rab32-subfamily proteins compete for binding to the ARM domain

The pulldowns imply that the Rab32-subfamily proteins bind to an identical site in the ARM domain. Further support for this model was obtained using competition studies (Figure 2(a)). His₆-tagged Rab29 and Rab32 were doped with untagged Rab38 prior to the pulldown of LRRK2. The results show a decrease in the levels of LRRK2, suggesting that Rab38 competes with Rab29 and Rab32. Rab8a was unable to compete for binding, suggesting that the ARM domain is indeed specific for the Rab32 subfamily (Suppl Figure S4). Isothermal

titration calorimetry was performed to characterize the affinity of Rab38:LRRK2 complexes (Figure 2(b)). The data reveal a stoichiometry of 1:1 and a K_d value of ~1 μM, which is typical of many Rab:effector complexes [12]. The GDP forms of Rabs are unable to bind under identical conditions using calorimetry or fluorescence experiments (Figure 2(b–e)), suggesting that LRRK2 is recognized by the Rab32 subfamily in a GTP-specific manner.

Rab32 and Rab29 were not amenable to ITC under the same experimental conditions due to protein precipitation at high concentrations, therefore an alternative method to study the interaction with LRRK2 was exploited. Using a fluorescently labelled (N-Methylanthraniloyl, mant) non-hydrolysable GTP analogue (mant-GppNHp) fluorescence anisotropy measurements were taken for Rab29 and Rab32. This method provided binding affinities to complement the ITC data, with equilibrium affinities all estimated in the low micromolar range (Figure 2(c)). Overall, the data support a model in which all members of the Rab32-subfamily bind to an identical site in the ARM domain of LRRK2 in a GTP dependent manner. The affinities from ITC and fluorescence assays are shown in Table 2.

Structural analyses of the GTP forms of the Rab32-subfamily

Given the GTP dependence of Rab32-subfamily binding to LRRK2, the crystal structures of the uncomplexed proteins were determined to provide structural insight into their active conformations. The X-ray structures of Rab32 and Rab38 bound to GTP were determined at 2.13Å and 1.79Å resolution, respectively (Figure 3, Table 3). Despite a Q67L mutation to stabilize GTP, Rab29 crystallized with GDP and the crystals diffracted to low resolution (data not shown), and this finding is consistent with previously observed destabilization of Rab29 harbouring the Q67L mutation [17]. Thus far, all attempts at crystallization of the GTP-bound structure have failed. A high-resolution (1.45Å) structure of Rab29 using the wild-type protein reveals a highly open conformation for switch 1 that involves a partial unwinding of the preceding α1 helix (Figure 3(a)). The unusual switch 1 conformation, which is partly α-helical (residues 34–40), is stabilized by crystallographic contacts (not shown). The crystal structure of Rab32(GDP) in complex with GtgE, a protease specific for the Rab32-subfamily, is also available [27]. In the switch 2 region of both these Rabs, a glutamate (Glu68 in Rab29, Glu86 in Rab32, Figure 3(a)) forms hydrogen bonds to the β-phosphate of GDP, effectively occupying the position of the gamma-phosphate.

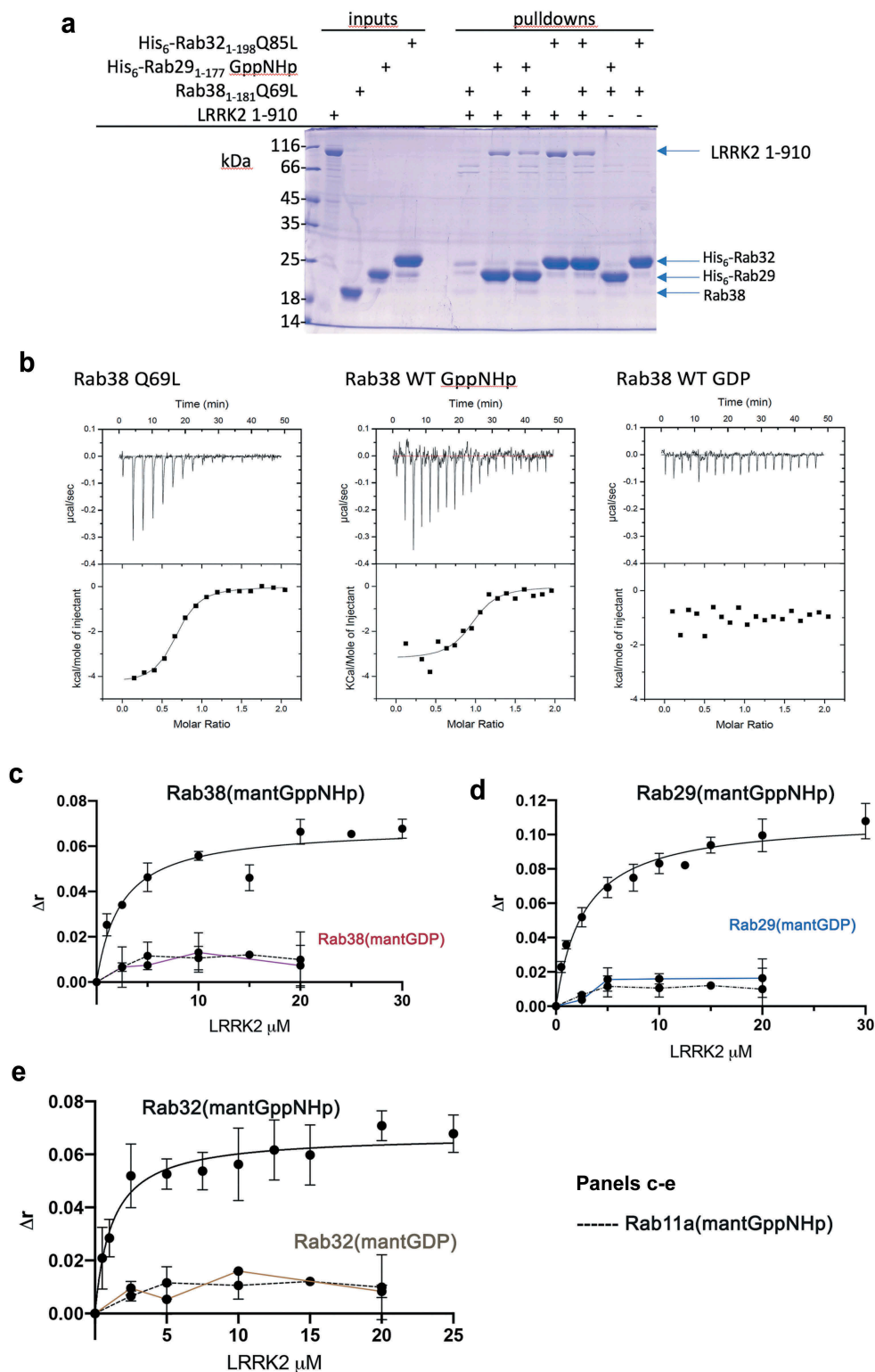


Figure 2. The Rab32 subfamily share a common LRRK2 binding site and interact in a GTP-dependent manner.

(a) Direct *in vitro* pull-down using His₆-Rab32/Rab29 as bait and LRRK2 1–910 as prey. A competition assay was performed by doping the pull-down samples with untagged Rab38. The presence of Rab38 results in a decrease in the levels of LRRK2 by SDS-PAGE analysis. (b) LRRK2:Rab38 interactions by isothermal titration calorimetry. Constitutively active Rab38 (Rab38 Q69L or Rab38 GppNHP) and inactive Rab38 GDP show the interaction with LRRK2 is dependent upon the GTP state of the Rab protein. Data fitting reveals that the $K_d = \sim 1\mu\text{M}$ and a stoichiometry of 1:1 for complex formation. (c–e) Fluorescence anisotropy titrations of Rab32 subfamily binding to LRRK2. The GTPases are associated with either mant-GppNHP or mant-GDP. As a further control, Rab11(mant-GppNHP) is also used to demonstrate Rab specificity.

Table 2. Binding affinities between the Rab32 subfamily and LRRK2 armadillo region.

	ITC K_d (μM)	Fluorescence K_d (μM)	ΔH (kcal/mol)	ΔS (cal/ mol/deg)
Rab38(GTP, QL)	1.2 ± 0.4	-	-4.3 ± 1	13 ± 4
Rab38(GTP, QL)	-	2.4 ± 1.5	-	-
Rab29(GppNHp, WT)	-	2.7 ± 0.8	-	-
Rab32(GTP, QL)	-	1.2 ± 0.5	-	-

All titrations of Rab GTPases were performed against the ARM domain of LRRK2 (1–552) as described in the **Materials and methods** section.

The active (GTP) conformations of Rab32 and Rab38 were analysed to understand the determinants of LRRK2 specificity (Figure 3(b–c)). In addition, a homology model of the ARM domain (1–552) was built to provide insight into possible Rab32-subfamily binding sites (Figure 3(d)). The structures of Rab32/38 are highly convergent in their switch 1 and 2 conformations, which reflects the high sequence similarities (67%) of the two proteins. The electrostatic surface features of Rab32/38 are identical at the junction of switch 1 and 2, which is generally the region that forms the interface with effector proteins [12]. The isoelectric point (pI) of the G-domains of the Rab32 subfamily is 8.4, while the pI of the ARM domain (1–552) of LRRK2 is 5.3, implying that there may be electrostatic complementarity in complex formation. Two distinct regions of positive charge are conserved in the Rab32-subfamily. In the structure of Rab38 (GTP), Arg39 in switch 1 and residues Arg77/Arg81 in switch 2 are surface exposed and potentially interact with LRRK2. These surface-exposed residues were targeted for mutagenesis, as they are unlikely to affect GTP binding or protein stability, and they are not fully conserved among the wider family of Rab GTPases (Figure 4). Homology modelling of the ARM domain of LRRK2 revealed clusters of negatively charged residues at several distinct surface patches (Figure 3(d)). These potential Rab/LRRK2 interfaces were further investigated through mutagenesis and binding assays.

Mutational studies reveal a candidate Rab:LRRK2 binding interface

Mutagenesis and pulldowns revealed that the single-site mutant R39Q of Rab38 reduced the binding to LRRK2 (Figure 5(a)). This switch 1 residue is conserved as Arg55 in Rab32 and Lys37 in Rab29. In contrast, a double Arg mutation in switch 2 of Rab38 (R77Q+R81Q) did not impact on LRRK2 binding. Mutations of a hydrophobic residue in switch 1 (I42A, I42E), which is widely exploited

by the Rab family as a binding interface, also did not significantly reduce LRRK2 binding (Suppl Figure S5). Fluorescence data confirmed the importance of the positive charge in switch 1 of Rab38 (Figure 5(b)), with binding to LRRK2 essentially abolished under the experimental conditions. The same effect was observed with the equivalent switch 1 mutation in Rab32 (R55Q) (Figure 5(f)). Surprisingly, mutation of the switch 1 lysine in Rab29 (K37Q) did not significantly alter LRRK2 binding (Figure 5(f)). In this case, the positively-charged switch 1 residue is not critical for the interaction and may suggest a distinct mode of binding for Rab29. Rab32/38 functions are associated with biogenesis of lysosome-related organelles in epithelial cells [28,29], while expression of Rab38 has recently been linked to pancreatic cancer [30]. LRRK2 is widely expressed in human tissues, but the links between Rab32/38 and LRRK2 *in vivo* requires further investigation. In particular, Rab38 is highly restricted in its tissue expression and is unlikely to be relevant to neuronal functions of LRRK2 in the brain.

Modelling of the ARM domain of LRRK2 suggested several surfaces with clusters of negative charges that could contribute to Rab32-subfamily interactions. Three predicted loops at residues 192–193, 317–342, and 386–392 were particularly prominent. These regions were mutated and subjected to pulldown studies with Rab38. The loop 317–342 is predicted to be a highly negatively-charged coiled coil (CC) and was eliminated and replaced with a short flexible linker (ΔCC mutant). In addition, multi-site mutants were generated to investigate the role of negatively-charged regions in binding to Rab GTPases: E192Q+E193Q = LRRK2^{Nmut}; D390N+D392N = LRRK2^{2mut}; D390N+E391Q+D392N = LRRK2^{3mut}; E386Q+D390N+E391Q+D392N = LRRK2^{4mut}. LRRK2^{2mut} was stably expressed and purified, and pulldowns revealed a decrease in binding to Rab29 and Rab38 (Figure 5(c), S4). This observation was validated by a reduction in the fluorescence signal of LRRK2^{2mut} vs LRRK2 WT binding to Rab29 (Figure 5(d)). Although LRRK2^{3mut} and LRRK2^{4mut} proteins were susceptible to proteolysis during purification, sufficient amounts of intact LRRK2 was purified to confirm that interactions with Rab38 were abolished (Figure 5(e)). In contrast, mutations in the loop 192–193, near the N-terminus of LRRK2 (LRRK2^{Nmut}) had no effects on the interactions with Rab38 (Figure S5B). Similarly, the ΔCC mutant was able to interact with Rab38 as effectively as the WT ARM domain (Figure S5C). Overall, these findings suggest that negatively charged residues in the region 386–392 of the ARM domain contribute to the binding interface with Rab GTPases.

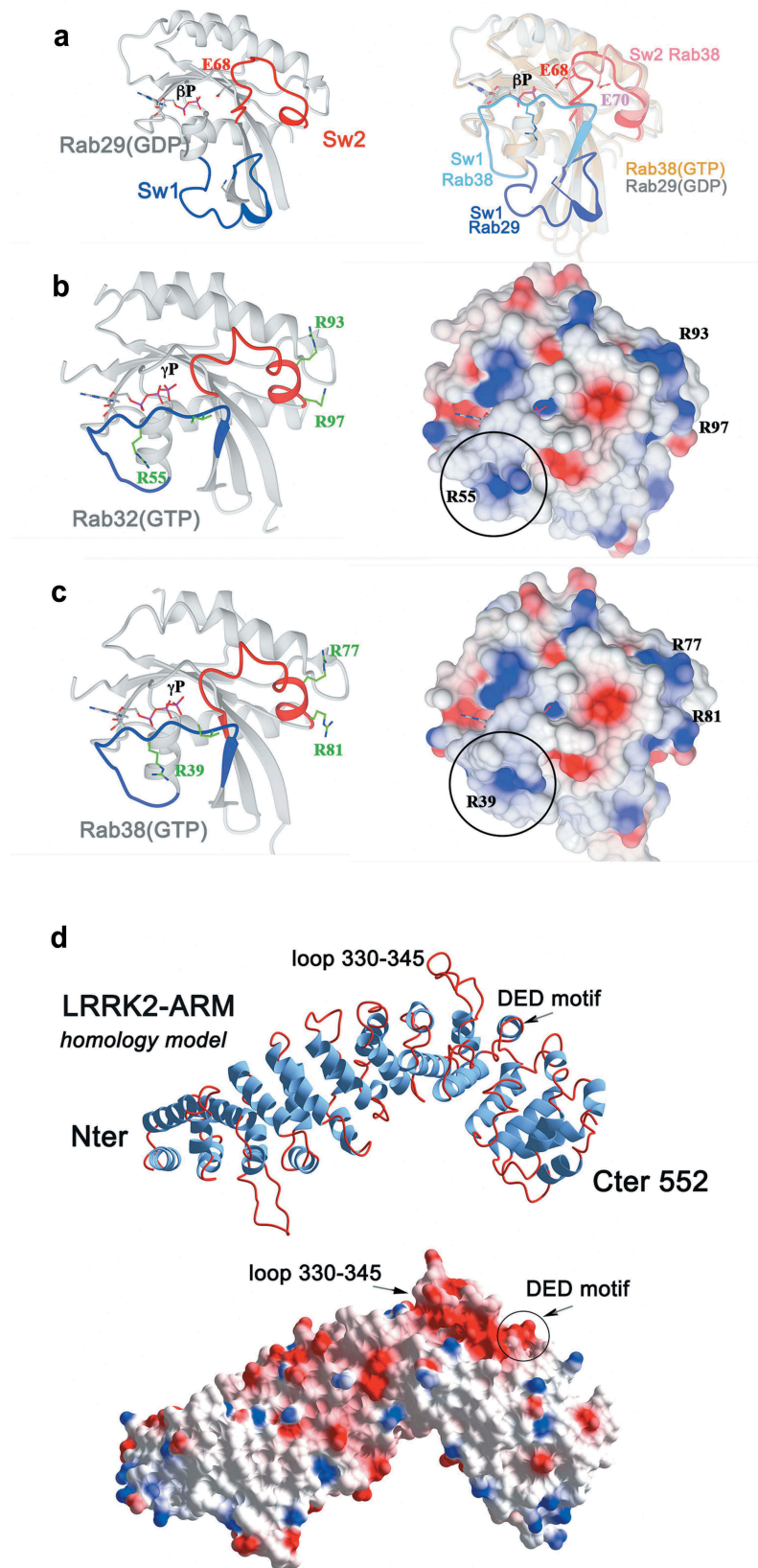


Figure 3. X-ray structures of the Rab32 subfamily of small GTPases.

(a) Structure of Rab29 reveals that a glutamate residue in Switch II forms hydrogen bonds to GDP in the nucleotide binding pocket and thereby occupies the position of the γ -phosphate of GTP. An overlay with active Rab38 illustrates the conformational shift in the Switch I between the active and inactive Rab GTPases. (b, c) The X-ray structures of Rab32 and Rab38 in their active (GTP) conformations, determined at 2.13 Å and 1.79 Å respectively, show highly convergent switch conformations and electrostatic surface features around the suspected effector binding interface. Positively charged residues within the switch regions that are surface exposed and may be important for complex formation are highlighted. (d) Homology modelling of the first 552 residues of the N-terminal LRRK2 armadillo repeats identifies distinct regions of negative charge that may represent the Rab32 subfamily binding site.

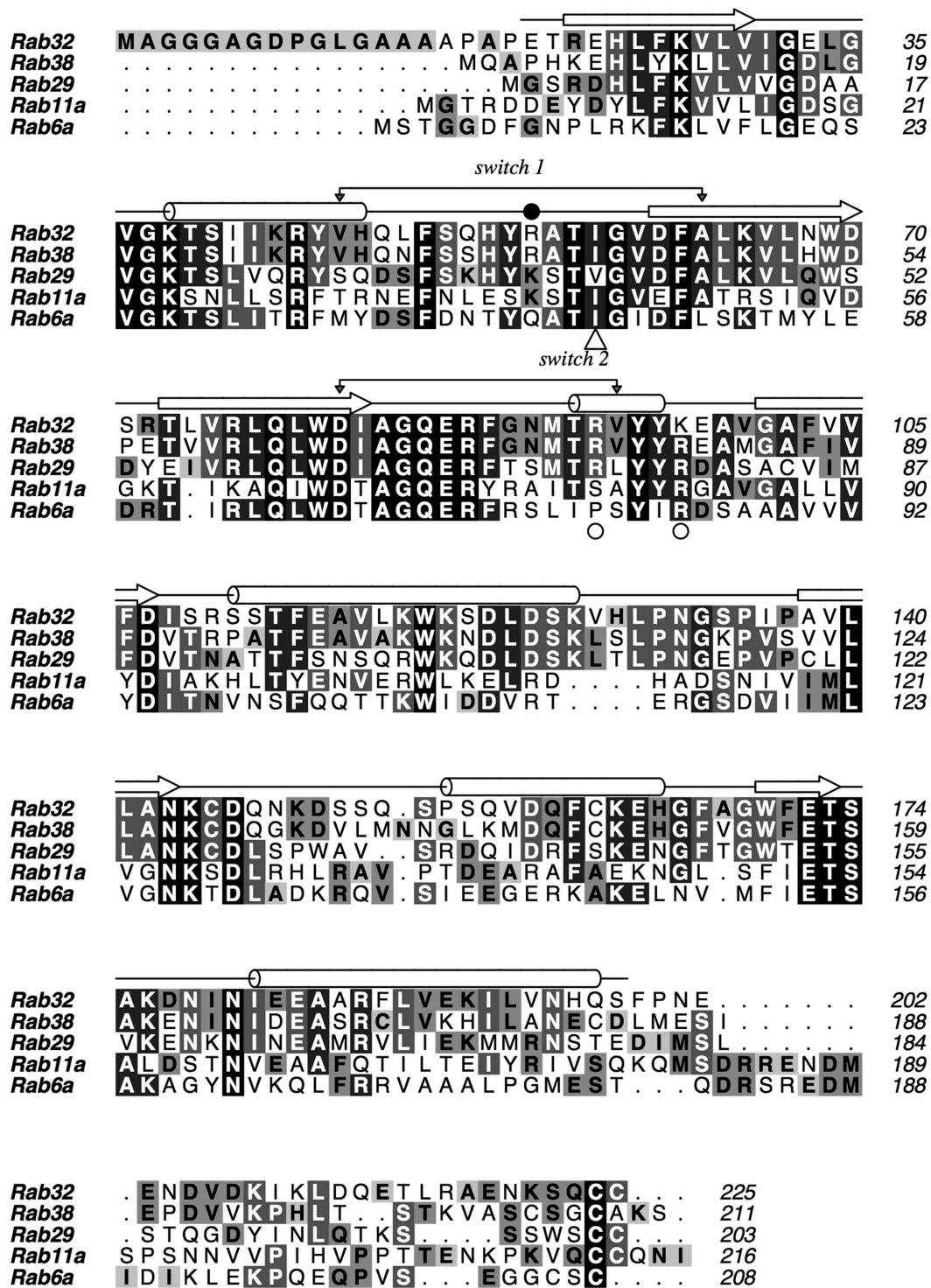


Figure 4. Sequence alignment of selected Rab GTPases. The secondary structure above the alignment corresponds to Rab32(GTP). The switch region of Rab32 is based on conformational differences with Rab32(GDP) upon superimposition of the structures. Filled circle indicates the position of the arginine mutations in switch 1 that reduce LRRK2 binding. The open circles and triangle indicate sites of mutations that have little or no effects on binding.

Discussion

The molecular mechanism by which Rab29 enhances the kinase activity of LRRK2 is a fascinating problem that is

central to an understanding of the biological role of LRRK2. In a previous study with GTP/GDP cycle-deficient mutants of Rab29 (T21N and Q67L), it was suggested that Rab29 binds in both GTP and GDP states

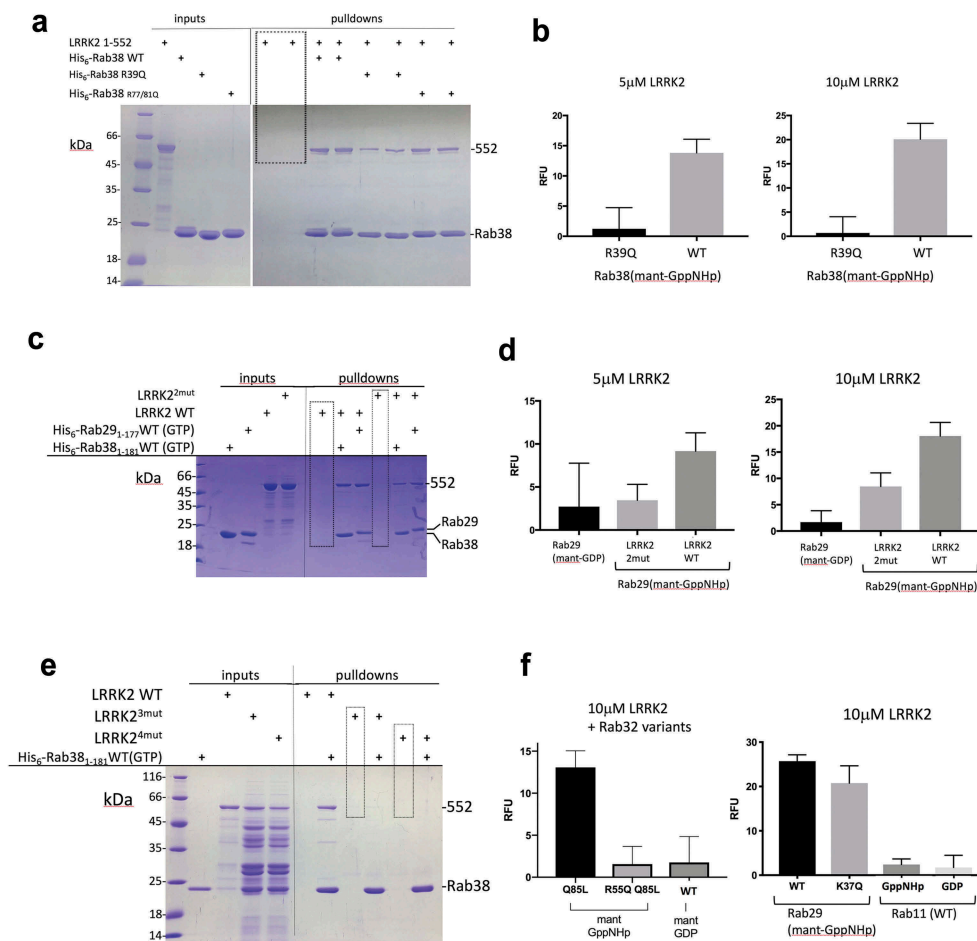


Figure 5. Mutational and biophysical analyses of the interactions between Rab32-subfamily proteins and the ARM domain of LRRK2. (a) Pull-downs of LRRK2 using His₆-Rab38. (b) Change in relative fluorescence (RFU) of Rab38 (R39Q) vs Rab38 WT at fixed concentrations of LRRK2. (c) Pull-downs of LRRK2^{2mut} (D390N+D392N) using His₆-Rab29. (d) Fluorescence-based assays reveal Rab29 binding to the ARM domain of LRRK2, and a reduction of binding to LRRK2^{2mut}. (e) Further mutagenesis of negatively charged loop (386–392) severely compromises binding to Rab38 (LRRK2^{3mut} = D390N+ E391Q+D392N; and LRRK2^{4mut} = E386Q+D390N+E391Q+D392N). (f) *Left*, fluorescence changes upon binding switch 1 mutant Rab32(R55Q) to LRRK2 (1–552). This variant includes the Q85L background (GTP stabilized). Therefore, Rab32 binding to LRRK2 is GTP dependent and utilizes the positive charge in switch 1. *Right*, a similar mutation in switch 1 of Rab29 does not have a significant effect. In this case, Rab29(K37Q) has the WT glutamine in switch 2, as the QL mutation renders the protein insoluble. However, Rab29 has been substituted with GppNHP to stabilize the GTP state.

[17,31]. However, these mutations appeared to generally destabilize Rab29 folding in their experiments, and the relative affinities of Rab29(GDP) and Rab29(GTP) were not clarified. GTP-bound Rab29 appears to be necessary for LRRK2 phosphorylation of Rab8/10 [18]. In this latter study, the QL-mutation in switch 2 of Rab29 destabilized the protein and reduced LRRK2 phosphorylation. A direct demonstration of Rab29(GTP) binding to LRRK2 is therefore lacking in the literature.

Here, we have clarified the nucleotide specificity using pure preparations of the Rab32-subfamily and shown that LRRK2 binds to the GTP conformation of these closely related small GTPases. WT Rab29 substituted with non-hydrolyzable GppNHP or excess GTP *in vitro* is stable and binds consistently to LRRK2.

Rab32 and Rab38 bind robustly, either as QL variants, or with GppNHP exchanged into wild-type proteins. We have identified a positively-charged residue in switch 1 of Rab32/38 that mediates interactions with LRRK2. ITC and equilibrium fluorescence titrations reveal a dissociation constant (K_d) of $\sim 1\text{--}3\ \mu\text{M}$ between Rab29/32/38 and LRRK2.

Rab29 has been characterized as both a substrate (one or both of Thr71/Ser72) and an upstream activator of LRRK2. Its role in recruitment of LRRK2 to Golgi is apparently not dependent on phosphorylation of its switch 2, since LRRK2 is still recruited in the presence of the kinase inhibitor, Mli-2[5]. Rab29 phosphorylation is currently assayed with a recombinant overexpression system – endogenous Rab29 phosphorylation has not yet been confirmed.

However, single-site mutants T71A and S72A retain the ability to activate LRRK2 in the context of mutant R1441G [14]. This appears consistent with our *in vitro* studies suggesting phosphorylation would not be necessary for binding to LRRK2. In contrast, Rab32 and Rab38 do not have a conserved Ser/Thr in their switch 2 region that could act as a substrate for LRRK2[5]. Since Rab32/38 clearly bind to LRRK2 in their GTP state, it is likely that phosphorylation of switch 2 is not required for binding to LRRK2 by the Rab32 subfamily.

The localization of the Rab29 binding site to the ANK domain of LRRK2 has recently been proposed [14,16]. Here, we provide strong evidence for a LRRK2 binding site on the ARM domain. A negatively-charged region that is presumed to be a loop that connects armadillo motifs from modelling studies (residues 386–392) contributes to Rab recognition. Our *in vitro* expression studies of the ARM-ANK region (1–910) reveal that mutations in the ANK domain likely destabilize the folding and stability of LRRK2. In previous cellular work, ANK mutations decreased overall kinase activity and were less stable in HEK293 cells, relative to wild-type LRRK2 [14]. A model that reconciles cellular data with *in vitro* binding studies is that ANK mutations disrupt the Rab32-subfamily binding site in the ARM domain. It is noteworthy that among the numerous mutations and deletions within the ARM domain that were generated, the only effects on Rab32-subfamily binding were imparted by Glu/Asp mutants in the loop 386–392. Interestingly, the ‘DED’ motif in this loop is highly conserved among mammalian LRRK2 sequences, but not generally in the animal kingdom (Suppl Figure S6).

In summary, these data provide a conceptual framework for investigating the molecular mechanism for Rab29-mediated activation of LRRK2 kinase activity. The GTP-dependence of the interaction is consistent with the recruitment of LRRK2 to Golgi compartments, and therefore, sub-cellular localization may contribute towards the increased phosphorylation of substrate Rab GTPases. It is fascinating that despite robust interactions with the G domains *in vitro*, full-length Rab32 and Rab38 do not significantly activate the kinase activity of LRRK2 in cells. Among the eleven additional Rabs surveyed, only Rab38 expression resulted in a modest increase in S1292 autophosphorylation in the context of the R1441G mutation of LRRK2[14]. However, the observed kinase activation was significantly less compared to Rab29 expression. It will be interesting to determine the molecular basis for Rab29 activation of LRRK2 with future structural and functional studies.

Acknowledgments

The authors wish to thank Dario Alessi (University of Dundee) and Suzanne Pfeffer (Stanford University) for their advice and

support. This work was supported by Science Foundation Ireland Principal Investigator Awards (grant number 12/IA/1239 to ARK). EM was supported by the Naughton Foundation through a Fellowship (Ireland/USA). Data were collected at the Northeastern Collaborative Access Team beamlines, which are funded by the National Institute of General Medical Sciences from the National Institutes of Health (P41 GM103403). This research used resources of the Advanced Photon Source, a U.S. Department of Energy (DOE) Office of Science User Facility operated for the DOE Office of Science by Argonne National Laboratory under Contract No. DE-AC02-06CH11357. The content is solely the responsibility of the authors and does not necessarily represent the official views of the National Institutes of Health. The authors also wish to thank Proxima-2A beamline staff for their assistance during data collection at the Soleil Synchrotron.

Disclosure statement

No potential conflict of interest was reported by the authors.

Funding

This work was supported by the Science Foundation Ireland [12/IA/1239] and the Naughton Foundation

ORCID

Emma McGrath  <http://orcid.org/0000-0002-7257-560X>
Amir R. Khan  <http://orcid.org/0000-0003-1176-6952>

References

- [1] Fahn S. Description of Parkinson's disease as a clinical syndrome. *Ann N Y Acad Sci.* 2003;991:1–14.
- [2] Schulte C, Gasser T. Genetic basis of Parkinson's disease: inheritance, penetrance, and expression. *Appl Clin Genet.* 2011;4:67–80.
- [3] Roosen DA, Cookson MR. LRRK2 at the interface of autophagosomes, endosomes and lysosomes. *Mol Neurodegener.* 2016;11:73.
- [4] Greggio E, Zambrano I, Kaganovich A, et al. The Parkinson disease-associated leucine-rich repeat kinase 2 (LRRK2) is a dimer that undergoes intramolecular autophosphorylation. *J Biol Chem.* 2008;283:16906–16914.
- [5] Steger M, Tonelli F, Ito G, et al. Phosphoproteomics reveals that Parkinson's disease kinase LRRK2 regulates a subset of Rab GTPases. *Elife.* 2016;5:12813.
- [6] Zimprich A, Biskup S, Leitner P, et al. Mutations in LRRK2 cause autosomal-dominant parkinsonism with pleomorphic pathology. *Neuron.* 2004;44:601–607.
- [7] Paisan-Ruiz C, Jain S, Evans EW, et al. Cloning of the gene containing mutations that cause PARK8-linked Parkinson's disease. *Neuron.* 2004;44:595–600.
- [8] Hui KY, Fernandez-Hernandez H, Hu J, et al. Functional variants in the LRRK2 gene confer shared effects on risk for Crohn's disease and Parkinson's disease. *Sci Transl Med.* 2018;10:eaa17795.

- [9] Bardien S, Lesage S, Brice A, et al. Genetic characteristics of leucine-rich repeat kinase 2 (LRRK2) associated Parkinson's disease. *Parkinsonism Relat Disord.* **2011**;17:501–508.
- [10] West AB, Cookson MR. Identification of bona-fide LRRK2 kinase substrates. *Mov Disord.* **2016**;31:1140–1141.
- [11] Hutagalung AH, Novick PJ. Role of Rab GTPases in membrane traffic and cell physiology. *Physiol Rev.* **2011**;91:119–149.
- [12] Khan AR, Menetrey J. Structural biology of Arf and Rab GTPases' effector recruitment and specificity. *Structure.* **2013**;21:1284–1297.
- [13] Steger M, Diez F, Dhekne HS, et al. Systematic proteomic analysis of LRRK2-mediated Rab GTPase phosphorylation establishes a connection to ciliogenesis. *Elife.* **2017**;6:e31012.
- [14] Purlyte E, Dhekne HS, Sarhan AR, et al. Rab29 activation of the Parkinson's disease-associated LRRK2 kinase. *Embo J.* **2018**;37:1–18.
- [15] Waschbusch D, Michels H, Strassheim S, et al. LRRK2 transport is regulated by its novel interacting partner Rab32. *PLoS One.* **2014**;9:e111632.
- [16] Alessi DR, Sammler E. LRRK2 kinase in Parkinson's disease. *Science.* **2018**;360:36–37.
- [17] Beilina A, Rudenko IN, Kaganovich A, et al. Unbiased screen for interactors of leucine-rich repeat kinase 2 supports a common pathway for sporadic and familial Parkinson disease. *Proc Natl Acad Sci U S A.* **2014**;111:2626–2631.
- [18] Liu Z, Bryant N, Kumaran R, et al. LRRK2 phosphorylates membrane-bound Rabs and is activated by GTP-bound Rab7L1 to promote recruitment to the trans-Golgi network. *Hum Mol Genet.* **2018**;27:385–395.
- [19] Heyduk T, Ma Y, Tang H, et al. Fluorescence anisotropy: rapid, quantitative assay for protein-DNA and protein-protein interaction. *Methods Enzymol.* **1996**;274:492–503.
- [20] Kabsch W. Xds. *Acta Crystallogr D Biol Crystallogr.* **2010**;66:125–132.
- [21] Evans P. Scaling and assessment of data quality. *Acta Crystallogr D Biol Crystallogr.* **2006**;62:72–82.
- [22] Hesketh GG, Perez-Dorado I, Jackson LP, et al. VARP is recruited on to endosomes by direct interaction with retromer, where together they function in export to the cell surface. *Dev Cell.* **2014**;29:591–606.
- [23] Adams PD, Afonine PV, Bunkoczi G, et al. PHENIX: a comprehensive Python-based system for macromolecular structure solution. *Acta Crystallogr D Biol Crystallogr.* **2010**;66:213–221.
- [24] Emsley P, Lohkamp B, Scott WG, et al. Features and development of Coot. *Acta Crystallogr D Biol Crystallogr.* **2010**;66:486–501.
- [25] Group CC. Molecular Operating Environment (MOE). 1010 Sherbooke St. West, Suite #910, Montreal, QC, Canada, H3A 2R7; **2018**.
- [26] Guaitoli G, Raimondi F, Gilsbach BK, et al. Structural model of the dimeric Parkinson's protein LRRK2 reveals a compact architecture involving distant inter-domain contacts. *Proc Natl Acad Sci U S A.* **2016**;113: E4357–4366.
- [27] Wachtel R, Brauning B, Mader SL, et al. The protease GtgE from *Salmonella* exclusively targets inactive Rab GTPases. *Nat Commun.* **2018**;9:44.
- [28] Aguilar A, Weber J, Boscher J, et al. Combined deficiency of RAB32 and RAB38 in the mouse mimics Hermansky-Pudlak syndrome and critically impairs thrombosis. *Blood Adv.* **2019**;3:2368–2380.
- [29] Bultema JJ, Di Pietro SM. Cell type-specific Rab32 and Rab38 cooperate with the ubiquitous lysosome biogenesis machinery to synthesize specialized lysosome-related organelles. *Small GTPases.* **2013**;4:16–21.
- [30] Li BY, He LJ, Zhang XL, et al. High expression of RAB38 promotes malignant progression of pancreatic cancer. *Mol Med Rep.* **2019**;19:909–918.
- [31] MacLeod DA, Rhinn H, Kuwahara T, et al. RAB7L1 interacts with LRRK2 to modify intraneuronal protein sorting and Parkinson's disease risk. *Neuron.* **2013**;77:425–439.